symmetry

MDPI

Article

Optimal Penetration Guidance Law for High-Speed Vehicles against an Interceptor with Modified Proportional Navigation Guidance

Lei Feng, Wang Lu *, Fenglin Wang, Fan Zhang and Qiangui Sun

Space Operate Lab, Beijing Institute of Tracking and Telecommunication Technology, Beijing 100094, China
* Correspondence: wanglu199310@163.com

Abstract: Aiming at the penetration problem of high-speed vehicles against a modified proportional guidance interceptor, a three-dimensional mathematical model of attack–defense confrontation between the high-speed vehicle and the interceptor is established in this paper. The modified proportional navigation guidance law of the interceptor is included in the model, and control constraints, pitch angle velocity constraints, and dynamic delay are introduced. Then, the performance index of the optimal penetration of high-speed vehicles is established. Under the condition of considering the 180-degree BTT control, the analytical solutions of the optimal speed roll angle and the optimal overload of high-speed vehicles are obtained according to symmetric Hamilton principle. The simulation results show that the overload switching times of high-speed vehicles to achieve optimal penetration are $N-1$, where N is the modified proportional guidance coefficient of the interceptor. When the maximum speed roll angle velocity is [60, 90] degrees per second, the penetration effect of high-speed vehicles is good. Finally, the optimal penetration guidance law proposed in this paper can achieve a miss distance of more than 5 m when the overload capacity ratio is 0.33.

Keywords: high-speed vehicles; modified proportional navigation guidance; optimal penetration guidance law; Hamilton principle

Citation: Feng, L.; Lu, W.; Wang, F.; Zhang, F.; Sun, Q. Optimal Penetration Guidance Law for High-Speed Vehicles against an Interceptor with Modified Proportional Navigation Guidance. *Symmetry* **2023**, *15*, 1337. https://doi.org/10.3390/sym15071337

Academic Editors: Alexander Zaslavski, Chuang Liu, Dong Ye and Haizhao Liang

Received: 4 April 2023
Revised: 15 June 2023
Accepted: 27 June 2023
Published: 30 June 2023

1. Introduction

Near space high-speed vehicle technology is an important milestone in the history of modern weapons and equipment. As the commanding height of science and technology, it greatly enriches the content of attack–defense confrontation in near space [1–4]. Aiming at the optimal penetration guidance problem of high-speed vehicles against a modified proportional guidance interceptor, this paper obtains the analytical solution of an optimal penetration strategy by introducing Hamilton's principle [5–7]. Hamilton's principle is based on the principle of minimum action, which indicates that the motion trajectory of an object in any time interval causes the action to obtain the extreme value. This means that in a system, the motion track of an object is the track that causes the action (i.e., the sum of the Lagrangian integral in the time interval) to obtain the extreme value. The optimal penetration strategy reflects a principle of stability and symmetry, which pursues a balance between the maximum expected miss distance and the minimum required energy.

Now, the research on the guidance of high-speed vehicles mainly focuses on re-entry guidance, trajectory optimization, etc. Zhang Konan et al. [8] solved the optimization of aircraft penetration parameters using the sequential quadratic programming method and obtained several typical penetration modes; however, the form is relatively simple. Wang Qing et al. [9] proposed a predictive correction guidance method to study the re-entry guidance problem of high-speed vehicles. The constraints of dynamic pressure, overload, heat flow, etc. are comprehensively considered to successfully avoid the no-fly circle, and the guidance and impact accuracy are high. Ming C et al. [10] effectively solved the trajectory planning problem under multiple constraints based on the pseudospectral method

and its improved method, but the pseudospectral method and its improved algorithm are highly dependent on the initial guess, and the algorithm iteration efficiency fluctuates. Wang Jianhua et al. [11] obtained pitch, yaw, and roll rate commands using the terminal sliding mode control method and the principle of zeroing the line-of-sight angular rate, and designed the guidance control in an integrated way; however, the target is a stationary ground target. Liu Qingkai et al. [12] introduced four elements to avoid the divergence of the Euler angle solution and improved the hit accuracy, but, again, for stationary targets.

However, the research on the guidance of high-speed vehicles against a modified proportional guidance interceptor is relatively scarce at home and abroad. It mainly includes the following: Rusnak, I. et al. [13] raised the issue of three-party pursuit and gave their respective action strategies based on simple assumptions. Perelman A. et al. [14] obtained the optimal guidance strategy for attack–defense confrontation based on linear differential game theory, but the obtained results only depend on their maximum mobility, which are conservative strategies. Kumar S. R. et al. [15] studied the cooperative guidance strategy for defense missiles and protected aircraft according to optimal control theory. The results show that the cooperative strategy can effectively protect aircraft and reduce the overload demand of defense missiles. Weiss M. et al. [16] studied the combined penetration attack guidance law of homing missiles and the cooperative guidance law of defense missiles and protected aircraft. However, their assumptions about the enemy were relatively simple in the derivation process, and their respective control saturation constraints were ignored. Gao Changsheng et al. [17] studied the trajectory design of a hypersonic glider to avoid a no-fly zone and divided the whole trajectory into several segments by introducing splicing points. However, the adaptability of splicing point selection needs to be strengthened. Li Jinglin et al. [18] studied the problem of terminal re-entry maneuver penetration and precision strikes for gliding high-speed vehicles. They established a multiobject, multisegment, and multiconstraint maneuver penetration trajectory optimization model and proposed an optimization strategy to deal with the shortcomings of the pseudospectral method, but it only aimed at stationary targets. Guo Hang et al. [19] designed a penetration guidance law to break the antiorbit interception situation based on the model predictive static planning algorithm for the penetration guidance problem of the cruise phase of air-breathing high-speed aircraft, making it impossible for the interceptor to achieve the intermediate and terminal guidance handover.

In recent years, the penetration guidance law considering reasonable penetration with a certain miss distance has gradually become a research hotspot. Based on the optimal control theory, Guo Hang et al. [20] studied the penetration guidance law for the target defense missile group and achieved the guidance effect of penetrating the defense missile and attacking the target under the situation of three-way attack–defense confrontation. In view of the problem of an air-breathing hypersonic vehicle penetrating multiple interceptors, Tian et al. [21] designed the optimal performance index of penetration with a certain miss distance, proposed the concept of a penetration window, and gave the penetration strategies and simulation effects of "one out of two" under different situations.

Aiming at the optimal penetration guidance problem of a near space high-speed vehicle against a modified proportional guidance interceptor, a three-dimensional mathematical model of attack–defense confrontation between the high-speed aircraft and the interceptor is established in this paper. The modified proportional guidance law of the interceptor is included in the model, and control constraints, speed roll angle speed constraints, and dynamic delay are introduced. Based on the performance index of the optimal penetration of the high-speed vehicle, and considering the 180° bank-to-turn (BTT) control of high-speed aircraft [19], the analytical solution of the optimal speed roll angle and optimal overload of the high-speed vehicle is obtained according to Hamilton's principle. The main contributions of the paper can be concluded as follows:

(a) Rather than using the proportional guidance law as in most other papers, the modified proportional guidance law of the interceptor is introduced, which is more challenging for the penetration strategy of the high-speed vehicles;

(b) The analytical solution of the optimal penetration strategy using a three-dimensional mathematical model of attack–defense confrontation is derived in this paper; while in most other papers, only the analytical expression of the penetration strategy in the plane is obtained;
(c) Different from the conventional analytical expression derivation in previous papers, the common constraints in engineering applications are further considered and the application-oriented optimal penetration strategy is obtained in this paper.

2. Scenarios and Mathematical Models of High-Speed Vehicle Penetration

For the application scenario of the approximate antiorbit interception of a typical high-speed vehicle, it is assumed that both the high-speed vehicle and interceptors have the characteristic of a first-order link autopilot. The interceptor adopts the modified proportional guidance method, and the moving target is always in the horizontal plane. The three-dimensional space attack–defense confrontation relationship is shown in Figure 1.

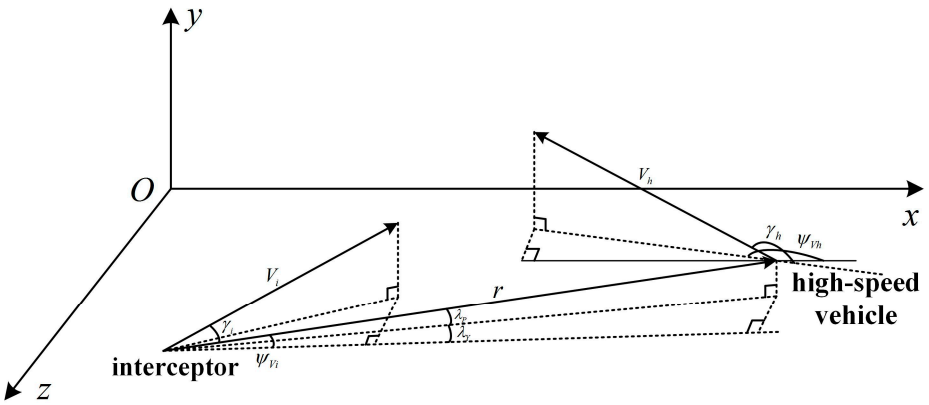

Figure 1. The relative kinematics of spatial attack and defense countermeasure.

Considering the angle of attack constraint of high-speed aircraft in the actual situation, it is assumed that it adopts the 180° BTT control mode and introduces the maximum speed roll angle speed constraint. The state vector of the overall mathematical problem is as follows:

$$x = \left\{ y, \dot{y}, z, \dot{z}, n_y, n_{yi}, n_{zi}, \gamma_{Vh} \right\}^T \tag{1}$$

The mathematical model can be expressed as follows:

$$\begin{cases} \dot{y} = \dot{y} \\ \ddot{y} = n_y g \cos \gamma_{Vh} - n_{yi} g \\ \dot{z} = \dot{z} \\ \ddot{z} = -n_y g \sin \gamma_{Vh} - n_{zi} g \\ \dot{n}_y = -\frac{1}{\tau_y} n_y + \frac{1}{\tau_y} n_{yc} \\ \dot{n}_{yi} = -\frac{1}{\tau_i} n_{yi} + \frac{1}{\tau_i} n_{yic} \\ \dot{n}_{zi} = -\frac{1}{\tau_i} n_{zi} + \frac{1}{\tau_i} n_{zic} \\ \dot{\gamma}_{Vh} = \mu \dot{\gamma}_{Vhmax} \end{cases} \tag{2}$$

where (y, z) is the relative coordinate of the high-speed aircraft and interceptor in the y-axis and z-axis; (n_{yi}, n_{zi}) is the actual overload of the interceptor in the y and z directions; (n_{yic}, n_{zic}) is the command overload of the interceptor in the y and z directions; (n_{yc}, n_y) are the command overload and actual overload of high-speed aircraft; γ_{Vh} is the speed roll angle of high-speed aircraft; μ is the speed roll angle speed equivalent command of high-speed aircraft; $\dot{\gamma}_{Vhmax}$ is the maximum speed roll angle velocity of the high-speed

aircraft; (τ_y, τ_i) is the dynamic time constant of the high-speed aircraft and interceptor; g is the acceleration of gravity. According to the modified proportional navigation method,

$$\begin{cases} n_{yic} = \frac{V_i N \dot{\lambda}_P}{g} + \frac{1}{2} n_y \cos \gamma_{Vh} \\ n_{zic} = -\frac{V_i N \dot{\lambda}_Y}{g} - \frac{1}{2} n_y \sin \gamma_{Vh} \end{cases} \tag{3}$$

where V_i is the interceptor speed; (λ_P, λ_Y) are the elevation angle and azimuth angle of the line of sight of the high-speed aircraft relative to the interceptor, respectively. Under the condition of approximate antiorbit, the following formula is applied:

$$\begin{cases} \lambda_P = y/r \\ \lambda_Y = -z/r \end{cases} \tag{4}$$

where r is the distance. Then, the angular speed of the line of sight is:

$$\begin{cases} \dot{\lambda}_P = \frac{y}{V_c(t_f - t)^2} + \frac{\dot{y}}{V_c(t_f - t)} \\ \dot{\lambda}_Y = -\frac{z}{V_c(t_f - t)^2} - \frac{\dot{z}}{V_c(t_f - t)} \end{cases} \tag{5}$$

where V_c and t_f are the approach speed and terminal time. They are applied in the following formula:

$$\begin{cases} V_c = V_h + V_i \\ t_f = r/V_c \end{cases} \tag{6}$$

Then, the state equation of the system mathematical model is:

$$\begin{cases} \dot{y} = \dot{y} \\ \ddot{y} = n_y g \cos \gamma_{Vh} - n_{yi} g \\ \dot{z} = \dot{z} \\ \ddot{z} = -n_y g \sin \gamma_{Vh} - n_{zi} g \\ \dot{n}_y = -n_y/\tau_y + n_{yc}/\tau_y \\ \dot{n}_{yi} = \frac{N'}{\tau_i g} \frac{y}{(t_f - t)^2} + \frac{N'}{\tau_i g} \frac{\dot{y}}{t_f - t} + \frac{1}{2\tau_i} n_y \cos \gamma_{Vh} - \frac{1}{\tau_i} n_{yi} \\ \dot{n}_{zi} = \frac{N'}{\tau_i g} \frac{z}{(t_f - t)^2} + \frac{N'}{\tau_i g} \frac{\dot{z}}{t_f - t} - \frac{1}{2\tau_i} n_y \sin \gamma_{Vh} - \frac{1}{\tau_i} n_{zi} \\ \dot{\gamma}_{Vh} = \mu \dot{\gamma}_{Vhmax} \end{cases} \tag{7}$$

where $N' = NV_i/V_c$ is the effective navigation ratio.

The performance index of the optimal penetration guidance problem is:

$$\begin{aligned} \mathrm{J} &= -\frac{1}{2} \mathbf{x}\left(t_f\right)^T \mathbf{Q} \mathbf{x}\left(t_f\right) + \frac{1}{2} \int_{t_0}^{t_f} \mathbf{u}^T \mathbf{R}_u \boldsymbol{\mu} dt \\ &= -\frac{1}{2} Q_{11} y^2\left(t_f\right) - \frac{1}{2} Q_{33} z^2\left(t_f\right) + \frac{1}{2} \int_{t_0}^{t_f} \mathbf{R}_u n_{yc}^2 dt \end{aligned} \tag{8}$$

The penetration command input of the high-speed aircraft is $\mathbf{u} = \left(n_{yc}, \mu\right)^{\mathrm{T}}$, and the instruction constraint is:

$$\begin{cases} 0 \le n_{yc} \le n_{\mathrm{hmax}} \\ |\mu| \le 1 \end{cases} \tag{9}$$

3. Solution of Optimal Penetration Guidance Law for High-Speed Vehicle

According to the mathematical model of the optimal penetration problem of high-speed aircraft, the optimal control quantity can be expressed as

$$\left\{n_{yc}^*, \gamma_{Vh}^*\right\} = \underset{\{n_{yc}^*, \gamma_{Vh}^*\}}{\operatorname{argmin}} \mathrm{J} \tag{10}$$

The Hamilton function is:

$$\begin{array}{l} \mathrm{H} = \frac{1}{2}\mathbf{u}^{\mathrm{T}}\mathbf{R}_{\mathrm{u}}\mathbf{u} + \boldsymbol{\lambda}^{\mathrm{T}}\mathrm{f}(\mathbf{x}, \mathbf{u}, \mathbf{v}) \\ = \mathrm{H}(\mathbf{x}, \boldsymbol{\lambda}) + \frac{1}{2}\mathbf{R}_{\mathrm{u}}\mathrm{n}_{yc}^2 + \frac{\lambda_5}{\tau_y}n_{yc} \\ +\lambda_2 n_y g\cos\gamma_{Vh} - \lambda_4 n_y g\sin\gamma_{Vh} \\ -\frac{\lambda_6 n_y \cos\gamma_{Vh}}{2\tau_i} - \frac{\lambda_7 n_y \sin\gamma_{Vh}}{2\tau_i} \end{array} \tag{11}$$

Considering $n_y \geq 0$, then γ_{Vh}, which minimizes the Hamilton function, should satisfy:

$$\begin{cases} \cos\gamma_{Vh}^* = \dfrac{-\left(\lambda_2 g + \frac{\lambda_6}{2\tau_i}\right)}{\sqrt{\left(\lambda_2 g + \frac{\lambda_6}{2\tau_i}\right)^2 + \left(\lambda_4 g + \frac{\lambda_7}{2\tau_i}\right)^2}} \\ \sin\gamma_{Vh}^* = \dfrac{\left(\lambda_4 g + \frac{\lambda_7}{2\tau_i}\right)}{\sqrt{\left(\lambda_2 g + \frac{\lambda_6}{2\tau_i}\right)^2 + \left(\lambda_4 g + \frac{\lambda_7}{2\tau_i}\right)^2}} \end{cases} \tag{12}$$

The governing equation is:

$$\frac{\partial H}{\partial \mathbf{u}} = 0 \Rightarrow n_{yc}^* = -\frac{\lambda_5}{R_u \tau_y} \tag{13}$$

The co-state equation is:

$$\begin{cases} \dot{\lambda}_1 = -\frac{N'\lambda_6}{\tau_i g}\frac{1}{\left(t_f - t\right)^2} \\ \dot{\lambda}_2 = -\lambda_1 - \frac{N'\lambda_6}{\tau_i g}\frac{1}{t_f - t} \\ \dot{\lambda}_3 = -\frac{N_1'\lambda_7}{\tau_i g}\frac{1}{\left(t_f - t\right)^2} \\ \dot{\lambda}_4 = -\lambda_3 - \frac{N_1'\lambda_7}{\tau_i g}\frac{1}{t_f - t} \\ \dot{\lambda}_5 = -\left(\lambda_2 g + \frac{\lambda_6}{2\tau_i}\right)\cos\gamma_{Vh} + \left(\lambda_4 g + \frac{\lambda_7}{2\tau_i}\right)\sin\gamma_{Vh} + \frac{\lambda_5}{\tau_y} \\ \dot{\lambda}_6 = \lambda_2 g + \frac{\lambda_6}{\tau_i} \\ \dot{\lambda}_7 = \lambda_4 g + \frac{\lambda_7}{\tau_i} \end{cases} \tag{14}$$

In order to solve the above equation conveniently, the following variable is introduced:

$$v = \left(t_f - t\right)/\tau_i \tag{15}$$

According to the method of Laplace transform, the co-state variable could be solved as follows:

① When $N' = 3$, the co-state variable is solved as follows:

$$\begin{cases} \lambda_1(v) = Q_{11} y\left(t_f\right)\mathrm{e}^{-v}(1 - v/2) \\ \lambda_2(v) = \tau_i Q_{11} y\left(t_f\right)\mathrm{e}^{-v}\left(v - v^2/2\right) \\ \lambda_3(v) = Q_{33} z\left(t_f\right)\mathrm{e}^{-v}(1 - v/2) \\ \lambda_4(v) = \tau_i Q_{33} z\left(t_f\right)\mathrm{e}^{-v}\left(v - v^2/2\right) \\ \lambda_6(v) = -\tau_i^2 g Q_{11} y\left(t_f\right)\mathrm{e}^{-v}\left(v^2/2 - v^3/6\right) \\ \lambda_7(v) = -\tau_i^2 g Q_{33} z\left(t_f\right)\mathrm{e}^{-v}\left(v^2/2 - v^3/6\right) \end{cases} \tag{16}$$

In addition, for λ_5, when $\tau_i \neq \tau_y$, the result is as follows:

$$\lambda_5(v) = \begin{cases} -\tau_i^2 g \mathrm{e}^{-\tau_i v/\tau_y} R[h(v) + c_1] \; 0 \le v \le \frac{9-\sqrt{33}}{2} \\ \tau_i^2 g \mathrm{e}^{-\tau_i v/\tau_y} R[h(v) + c_2] \; \frac{9-\sqrt{33}}{2} < v < \frac{9+\sqrt{33}}{2} \\ -\tau_i^2 g \mathrm{e}^{-\tau_i v/\tau_y} R[h(v) + c_3] \; v \ge \frac{9+\sqrt{33}}{2} \end{cases} \tag{17}$$

where $R = \sqrt{Q_{11}^2 y^2\left(t_f\right) + Q_{33}^2 z^2\left(t_f\right)}$,

$$\begin{cases} h(v) = \frac{\tau_i}{\tau_i - \tau_f} \mathrm{e}^{\frac{\tau_i - \tau_y}{\tau_y} v} \left(v - \frac{3}{4}v^2 + \frac{1}{12}v^3\right) + \left(\frac{\tau_i}{\tau_i - \tau_f}\right)^2 \left[1 - \mathrm{e}^{\frac{\tau_i - \tau_y}{\tau_y} v} \left(1 - \frac{3}{2}v + \frac{1}{4}v^2\right)\right] \\ \quad + \left(\frac{\tau_i}{\tau_i - \tau_f}\right)^3 \left(\mathrm{e}^{\frac{\tau_i - \tau_y}{\tau_y} v} \frac{v-3}{2} + \frac{3}{2}\right) - \frac{1}{2}\left(\frac{\tau_i}{\tau_i - \tau_f}\right)^4 \left(\mathrm{e}^{\frac{\tau_i - \tau_y}{\tau_y} v} - 1\right) \\ c_1 = 0 \\ c_2 = -2h\left(\frac{9-\sqrt{33}}{2}\right) \\ c_3 = 2\left[h\left(\frac{9-\sqrt{33}}{2}\right) - h\left(\frac{9+\sqrt{33}}{2}\right)\right] \end{cases} \tag{18}$$

In particular, when $\tau_i = \tau_y$, the result is as follows:

$$\lambda_5(v) = \begin{cases} -\tau_i^2 g \mathrm{e}^{-v} R[h\prime(v) + c_1] \; 0 \le v \le \frac{9-\sqrt{33}}{2} \\ \tau_i^2 g \mathrm{e}^{-v} R[h\prime(v) + c_2] \; \frac{9-\sqrt{33}}{2} < v < \frac{9+\sqrt{33}}{2} \\ -\tau_i^2 g \mathrm{e}^{-v} R[h\prime(v) + c_3] \; v \ge \frac{9+\sqrt{33}}{2} \end{cases} \tag{19}$$

where

$$h'(v) = \frac{1}{2}v^2 - \frac{1}{4}v^3 + \frac{1}{48}v^4 \tag{20}$$

② When N'= 4, the co-state variables are as follows:

$$\begin{cases} \lambda_1(v) = Q_{11} y\left(t_f\right) \mathrm{e}^{-v}\left(1 - v + v^2/6\right) \\ \lambda_2(v) = \tau_i Q_{11} y\left(t_f\right) \mathrm{e}^{-v}\left(v - v^2 + v^3/6\right) \\ \lambda_3(v) = Q_{33} z\left(t_f\right) \mathrm{e}^{-v}\left(1 - v + v^2/6\right) \\ \lambda_4(v) = \tau_i Q_{33} z\left(t_f\right) \mathrm{e}^{-v}\left(v - v^2 + v^3/6\right) \\ \lambda_6(v) = -\tau_i^2 g Q_{11} y\left(t_f\right) \mathrm{e}^{-v}\left(v^2/2 - v^3/3 + v^4/24\right) \\ \lambda_7(v) = -\tau_i^2 g Q_{33} z\left(t_f\right) \mathrm{e}^{-v}\left(v^2/2 - v^3/3 + v^4/24\right) \end{cases} \tag{21}$$

In addition, for λ_5, when $\tau_i \neq \tau_y$, the result is as follows:

$$\lambda_5(v) = \begin{cases} -\tau_i^2 g \mathrm{e}^{-\tau_i v/\tau_y} R[k(v) + d_1] \; 0 \le v \le 6 - 2\sqrt{6} \\ \tau_i^2 g \mathrm{e}^{-\tau_i v/\tau_y} R[k(v) + d_2] \; 6 - 2\sqrt{6} < v < 4 \\ -\tau_i^2 g \mathrm{e}^{-\tau_i v/\tau_y} R[k(v) + d_3] \; 4 \le v \le 6 + 2\sqrt{6} \\ \tau_i^2 g \mathrm{e}^{-\tau_i v/\tau_y} R[k(v) + d_4] \; v > 6 + 2\sqrt{6} \end{cases} \tag{22}$$

where

$$\begin{cases} k(v) = \frac{\tau_i}{\tau_i-\tau_f}\mathrm{e}^{\frac{\tau_i-\tau_y}{\tau_y}v}\left(v-\frac{5}{4}v^2+\frac{1}{3}v^3-\frac{1}{48}v^4\right)+\left(\frac{\tau_i}{\tau_i-\tau_f}\right)^2\left[1-\mathrm{e}^{\frac{\tau_i-\tau_y}{\tau_y}v}\left(1-\frac{5}{2}v+v^2-\frac{1}{12}v^3\right)\right] \\ \quad +\left(\frac{\tau_i}{\tau_i-\tau_f}\right)^3\left[\frac{5}{2}-\mathrm{e}^{\frac{\tau_i-\tau_y}{\tau_y}v}\left(\frac{5}{2}-2v+\frac{1}{4}v^2\right)\right]+\left(\frac{\tau_i}{\tau_i-\tau_f}\right)^4\left[2-\left(2-\frac{1}{2}v\right)\mathrm{e}^{\frac{\tau_i-\tau_y}{\tau_y}v}\right] \\ \quad -\frac{1}{2}\left(\frac{\tau_i}{\tau_i-\tau_f}\right)^5\left[\mathrm{e}^{\frac{\tau_i-\tau_y}{\tau_y}v}-1\right] \\ d_1 = 0 \\ d_2 = -2\cdot k\left(6-2\sqrt{6}\right) \\ d_3 = -2\cdot\left[k\left(6-2\sqrt{6}\right)-k(4)\right] \\ d_4 = -2\cdot\left[k\left(6-2\sqrt{6}\right)-k(4)+k\left(6+2\sqrt{6}\right)\right] \end{cases} \tag{23}$$

In particular, when $\tau_i = \tau_y$, the result is as follows:

$$\lambda_5(v) = \begin{cases} -\tau_i^2 g\mathrm{e}^{-v}R[k\prime(v)+d_1] & 0 \le v \le 6-2\sqrt{6} \\ \tau_i^2 g\mathrm{e}^{-v}R[k\prime(v)+d_2] & 6-2\sqrt{6} < v < 4 \\ -\tau_i^2 g\mathrm{e}^{-v}R[k\prime(v)+d_3] & 4 \le v \le 6+2\sqrt{6} \\ \tau_i^2 g\mathrm{e}^{-v}R[k\prime(v)+d_4] & v > 6+2\sqrt{6} \end{cases} \tag{24}$$

where

$$k'(v) = \frac{1}{2}v^2 - \frac{5}{12}v^3 + \frac{1}{12}v^4 - \frac{1}{240}v^5 \tag{25}$$

After obtaining the co-state variable $\boldsymbol{\lambda}$, the optimal speed roll angle γ_{Vh}^* can be expressed as follows:

$$\begin{cases} \cos\gamma_{Vh}^* = \begin{cases} -\mathrm{sign}\left(v-\frac{3}{4}v^2+\frac{1}{12}v^3\right)\frac{Q_{11}y(t_f)}{R} & \left(N_1'=3\right) \\ -\mathrm{sign}\left(v-\frac{4}{5}v^2+\frac{1}{3}v^3-\frac{1}{48}v^4\right)\frac{Q_{11}y(t_f)}{R} & \left(N_1'=4\right) \end{cases} \\ \sin\gamma_{Vh}^* = \begin{cases} \mathrm{sign}\left(v-\frac{3}{4}v^2+\frac{1}{12}v^3\right)\frac{Q_{33}z(t_f)}{R} & \left(N_1'=3\right) \\ \mathrm{sign}\left(v-\frac{4}{5}v^2+\frac{1}{3}v^3-\frac{1}{48}v^4\right)\frac{Q_{33}z(t_f)}{R} & \left(N_1'=4\right) \end{cases} \end{cases} \tag{26}$$

where $\mathrm{sign}(\cdot)$ is the symbolic function.

Considering the need of high-speed aircraft to penetrate with as much miss distance as possible, the control constraints are considered in the performance index function $(Q_{11}, Q_{33}) \gg \mathbf{R}_\mathrm{u}$. Thus,

$$n_{yc}^* = n_{\mathrm{hmax}} \tag{27}$$

When $y\left(t_f\right)$ and $z\left(t_f\right)$ are determined, the optimal speed roll angle γ_{Vh}^* determines the "optimal penetration plane", and its switching is related to v (i.e., the remaining time). From a practical point of view, the normal operation of the high-speed aircraft engine requires that its flight dynamic pressure should be kept within a certain range. Therefore, maneuvering in the vertical plane will easily lead to the shutdown of the engine, which will cause the aircraft to stall and make it easier to intercept. Thus, the "optimal penetration plane" is simplified as a horizontal plane. In order to make full use of the position deviation in the z direction at the initial time with the least energy consumption, we have:

$$\mathrm{sign}\left[z\left(t_f\right)\right] = \mathrm{sign}[z(t_0)] \tag{28}$$

Then, the expression of the optimal velocity roll angle γ_{Vh}^* can be obtained as:

$$\gamma_{Vh}^* = \arcsin\begin{cases} \mathrm{sign}\left(v-\frac{3}{4}v^2+\frac{1}{12}v^3\right)\mathrm{sign}[z(t_0)] & \left(N_1'=3\right) \\ \mathrm{sign}\left(v-\frac{4}{5}v^2+\frac{1}{3}v^3-\frac{1}{48}v^4\right)\mathrm{sign}[z(t_0)] & \left(N_1'=4\right) \end{cases} \tag{29}$$

4. Simulation and Verification of Optimal Penetration Guidance Law for High-Speed Vehicle

We chose MATLAB as the simulation platform and the Simulink module was used to build the simulation system. The simulation parameter settings in typical scenarios are shown in Table 1. The initial situation of the simulation is illustrated by Figure 1.

Table 1. Values of simulation parameters for optimal penetration guidance law.

Parameter	Symbol	Unit	Value
Initial position of interceptor	/	/	(0, 0, 0)
Interceptor speed	V_i	km/s	data
Initial position of target	r	km	(30, 0, 0)
First-order time constant	(τ_i, τ_y)	s	(0.5, 0.5)
Maximum speed roll angle velocity of high-speed aircraft	$\dot{\gamma}_{Vhmax}$	deg/s	60
Speed of high-speed aircraft	V_h	km/s	1.5
Maximum usable overload of interceptor	n_{imax}	/	6
Maximum usable overload of high-speed aircraft	n_{hmax}	/	2
Corrected proportional guidance coefficient of interceptor	N	/	3

Under the typical interception situationof approximate reverse orbit, the flight paths of the high-speed aircraft and interceptor are shown in Figures 2 and 3. The change in the speed roll angle of the high-speed aircraft is shown in Figure 4, and the normal overload of the high-speed aircraft and interceptor is shown in Figure 5.

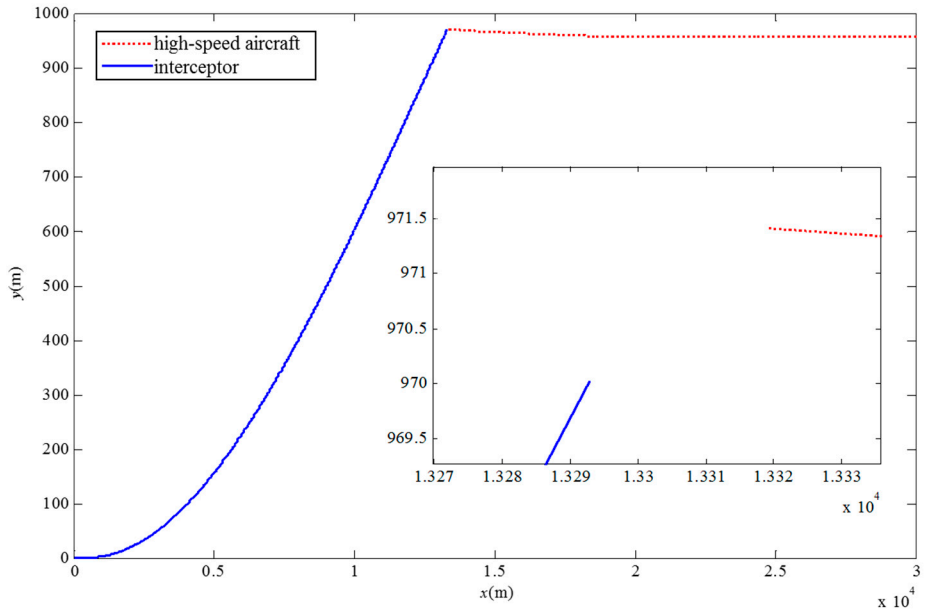

Figure 2. The longitudinal plane trajectory of high-speed aircraft and interceptor.

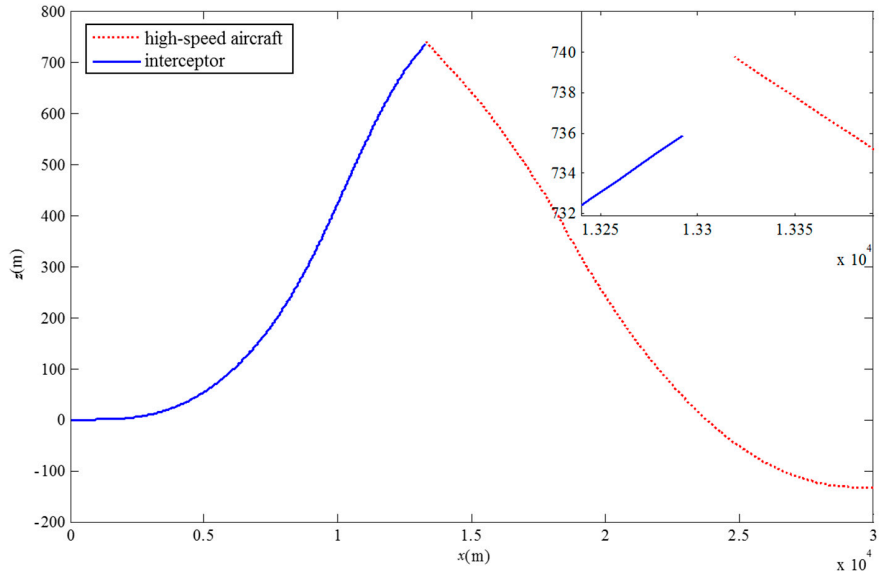

Figure 3. The lateral plane trajectory of high-speed aircraft and interceptor.

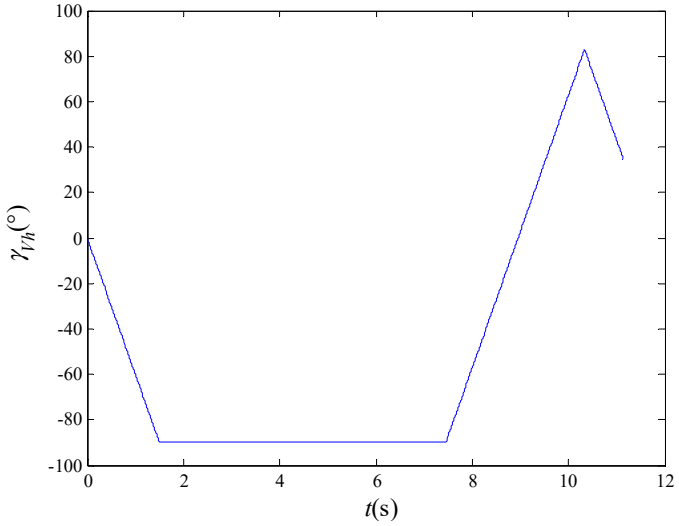

Figure 4. The change in speed roll angle of high-speed aircraft with time.

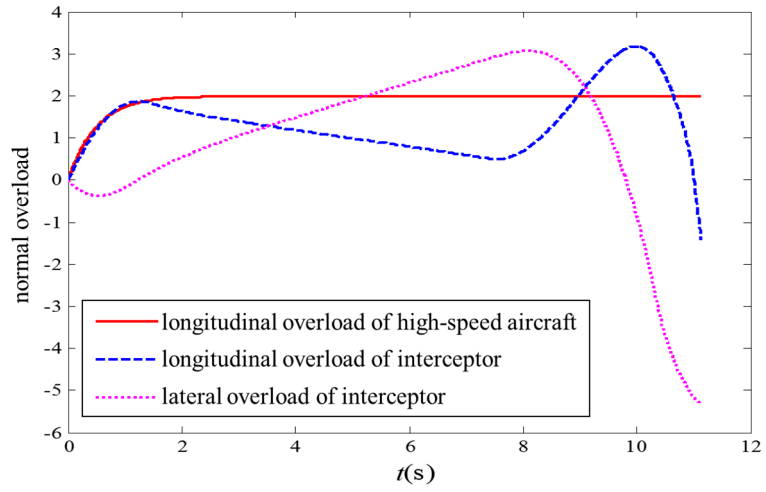

Figure 5. The normal overload change of high-speed aircraft and interceptor.

The Monte Carlo shooting simulation takes the initial longitudinal and azimuth line of sight angles (λ_{P0} and λ_{Y0}) as random variables, and they obeyed a uniform distribution of $U\left(0,(4/57.3)^2/12\right)$. In addition, 5000 shooting simulation runs were carried out for each case. The average miss distances at different maximum speed roll angle speeds $\dot{\gamma}_{Vhmax}$ of the high-speed aircraft are shown in Table 2.

Table 2. Simulation results of Monte Carlo shooting.

Parameter	Unit	Value		
Maximum speed roll angle velocity of high-speed aircraft, $\dot{\gamma}_{\mathrm{Vhmax}}$	°/s	30	60	75
Miss distance	m	0.625	3.431	3.172
Maximum speed roll angle velocity of high-speed aircraft, $\dot{\gamma}_{\mathrm{Vhmax}}$	°/s	90	120	150
Miss distance	m	2.156	1.316	1.508
Maximum speed roll angle velocity of high-speed aircraft, $\dot{\gamma}_{\mathrm{Vhmax}}$	°/s	180	240	300
Miss distance	m	1.873	2.348	2.791
Maximum speed roll angle velocity of high-speed aircraft, $\dot{\gamma}_{\mathrm{Vhmax}}$	°/s	360	720	∞
Miss distance	m	3.092	4.428	5.217

From the above simulation results, the following conclusions can be drawn:

(1) The overload switching times of high-speed aircraft to achieve optimal penetration is $N-1$, where N is the modified proportional guidance coefficient of interceptor;
(2) When $\dot{\gamma}_{Vhmax} \in \{60,\ 90\}(^\circ/\mathrm{s})$, the speed roll angle of the high-speed aircraft can enable its overload command to complete just one switch, which can produce a larger normal distance to penetrate; thus, the average miss distance is larger, and a better penetration effect is achieved;
(3) When $\dot{\gamma}_{Vhmax} \in \{90,\ 240\}(^\circ/\mathrm{s})$, the variation range of the speed roll angle γ_{Vh} of the high-speed aircraft is further increased, but the second switch cannot be completed effectively, which leads to the failure to fully utilize the mobility at the terminal time, and the penetration miss distance becomes smaller;
(4) When the speed roll angle speed constraint exceeds 240°/s, the penetration miss distance gradually approaches the penetration effect without the maximum speed roll angle speed constraint;
(5) From the perspective of high-speed aircraft penetration, the proposed optimal penetration strategy can achieve a miss distance of more than 5 m when the overload capacity ratio is 0.33.

5. Conclusions

On the basis of three-dimensional attack–defense confrontation, the optimal penetration guidance strategy for high-speed vehicles against an interceptor with modified proportional navigation guidance is proposed according to Hamilton's principle. The maximum speed roll angle velocity limit, the maximum available overload, and dynamic delay were introduced to verify the performance of the proposed penetration guidance strategy for the high-speed vehicles in a sense of a physical application. The Monte Carlo simulation showed that the proposed optimal penetration guidance law can successfully penetrate the modified proportional guidance interceptor when the overload capacity is weak, which guarantees the penetration of the high-speed vehicle with a desirable miss distance larger than 5 m. As a result, the optimal penetration guidance strategy of high-speed aircraft proposed in this paper can effectively deal with the modified proportional guidance interceptor, which provides a new idea and reference for the penetration guidance of high-speed vehicles in the future.

Author Contributions: Conceptualization, L.F. and W.L.; methodology, L.F. and F.W.; software, W.L.; formal analysis, F.Z; investigation, F.Z.; writing—original draft preparation, L.F.; writing—review and editing, W.L.; supervision, Q.S. All authors have read and agreed to the published version of the manuscript.

Funding: This research received no external funding.

Data Availability Statement: No new data were created or analyzed in this study. Data sharing is not applicable to this article.

Conflicts of Interest: The authors declare no conflict of interest.

References

1. Li, G.Z.; Yu, T.C.; Lai, Z.H. Inspiration of American X-51A hypersonic vehicle's development. *Aerodyn. Missile J.* **2014**, *5*, 5–8.
2. Wu, M.Y.; He, X.J.; Qiu, Z.M.; Chen, Z.H. Guidance law of interceptors against a high-speed maneuvering target based on deepQ-Network. *Trans. Inst. Meas. Control* **2022**, *44*, 1373–1387. [CrossRef]
3. Shen, Z.P.; Yu, J.L.; Dong, X.W.; Hua, Y.Z.; Ren, Z. Penetration trajectory optimization for the hypersonic gliding vehicle encountering two interceptors. *Aerosp. Sci. Technol.* **2022**, *121*, 107363. [CrossRef]
4. Jiang, L.; Nan, Y.; Zhang, Y.; Li, Z.H. Anti-Interception Guidance for Hypersonic Glide Vehicle: A Deep Reinforcement Learning Approach. *Aerospace* **2022**, *9*, 424. [CrossRef]
5. Tu, X.B.; Wang, Q.; Tang, Y.F. Highly Efficient Numerical Integrator for the Circular Restricted Three-Body Problem. *Symmetry* **2022**, *14*, 1769. [CrossRef]
6. Li, X.; Zhang, X.L.; Zhou, Z.H. Free Vibration Analysis of a Spinning Composite Laminated Truncated Conical Shell under Hygrothermal Environment. *Symmetry* **2022**, *14*, 1369. [CrossRef]
7. Postavaru, O.; Toma, A. Symmetries for Nonconservative Field Theories on Time Scale. *Symmetry* **2021**, *13*, 552. [CrossRef]
8. Zhang, K.N.; Zhou, H.; Chen, W.C. Trajectory planning for hypersonic vehicle with multiple constraints and multiple maneuvering penetration strategies. *J. Ballist.* **2012**, *24*, 85–90.
9. Wang, Q.; Mo, H.D.; Wu, Z.D.; Dong, C.Y. Predictive reentry guidance for hypersonic vehicles considering no-fly zone. *J. Harbin Inst. Technol.* **2015**, *47*, 104–109.
10. Ming, C.; Sun, R.S.; Bai, H.Y.; Yan, D.W. Climb trajectory optimization with multiple constraints for air-breathing supersonic missile. *J. Astronaut.* **2016**, *37*, 1063–1071.
11. Wang, J.H.; Liu, L.H.; Tang, G.J. Guidance and attitude control system design for hypersonic vehicle in dive phase. *J. Astronaut.* **2016**, *37*, 964–973.
12. Liu, Q.K.; Chen, J.; Wang, L.X.; Qin, W.W.; Zhang, G.H. Guidance and control design for hypersonic vehicle in dive phase. *Mod. Def. Technol.* **2017**, *45*, 74–81.
13. Rusnak, I. The lady, the bandits and the body-guards—A two team dynamic game. In Proceedings of the 16th IFAC World Congress, Prague, Czech Republic, 4–8 July 2005; pp. 441–446.
14. Perelman, A.; Shima, T.; Rusnak, I. Cooperative differential games strategies for active aircraft protection from a homing missile. *J. Guid. Control Dyn.* **2011**, *34*, 761–773. [CrossRef]
15. Kumar, S.R.; Shima, T. Cooperative nonlinear guidance strategies for aircraft defense. *J. Guid. Control Dyn.* **2017**, *40*, 124–138. [CrossRef]
16. Weiss, M.; Shima, T.; Castaneda, D.; Rusnak, I. Combined and cooperative minimum-effort guidance algorithms in an active aircraft defense scenario. *J. Guid. Control Dyn.* **2017**, *40*, 1241–1254. [CrossRef]
17. Gao, C.S.; Chen, E.K.; Jing, W.X. Maneuver evasion trajectory optimization for hypersonic vehicles. *J. Harbin Inst. Technol.* **2017**, *49*, 16–21.
18. Li, J.L.; Chen, W.C.; Min, C.W. Terminal hypersonic trajectory modeling and optimization for maneuvering penetration and precision strike. *J. Beijing Univ. Aeronaut. Astronaut.* **2018**, *44*, 556–567.
19. Guo, H.; Fu, W.X.; Fu, B.; Chen, K.; Yan, J. Penetration Trajectory Programming for Air-Breathing Hypersonic Vehicles During the Cruise Phase. *J. Astronaut.* **2017**, *38*, 287–295.
20. Guo, H.; Fu, W.X.; Fu, B.; Chen, K.; Yan, J. Smart Homing Guidance Strategy with Control Saturation Against a Cooperative Target-Defender Team. *J. Syst. Eng. Electron.* **2019**, *30*, 366–383.
21. Yan, T.; Cai, Y.L.; Xu, B. Evasion guidance algorithms for air-breathing hypersonic vehicles in three-player pursuit-evasion games. *Chin. J. Aeronaut.* **2020**, *33*, 3423–3436. [CrossRef]